Photochromic conversion in a red/green cyanobacteriochrome from Synechocystis PCC6803: quantum yields in solution and photoswitching dynamics in living E.coli cells

Journal Name

Dynamic Article Links ►

Cite this: DOI: 10.1039/c0xx00000x

www.rsc.org/xxxxxx

ARTICLE TYPE

Photochromic conversion in a red/green cyanobacteriochrome from *Synechocystis* PCC6803: quantum yields in solution and photoswitching dynamics in living *E.coli* cells

Francesca Pennacchietti,[a] Aba Losi,[b] Xiu-ling Xu,[c] Kai-hong Zhao,[d] Wolfgang Gärtner,[c] Cristiano Viappiani,[b,e] Francesca Cella,[a] Alberto Diaspro[a,f] and Stefania Abbruzzetti*[e,g]

Received (in XXX, XXX) Xth XXXXXXXXX 20XX, Accepted Xth XXXXXXXXX 20XX
DOI: 10.1039/b000000x

The protein encoded by the gene *slr1393* from the cyanobacterium *Synechocystis* sp. PCC6803 (Slr1393) is composed of three GAF domains, a PAS domain, and a histidine kinase motif. The third GAF domain (referred to as GAF3) was previously characterized as the sole domain in this protein able to carry phycocyanobilin (PCB) as chromophore and to accomplish photochemistry. GAF3 shows photochromicity, able to switch between a red-absorbing parental state ($GAF3_R$, λ_{max} = 649 nm) and a green-absorbing photoproduct state ($GAF3_G$, λ_{max} = 536 nm) upon appropriate irradiation. In this study we have determined the photochemical quantum yields for the interconversion between both forms using two methods: an "absolute" method and a reference-based control. The latter is a comparative procedure which exploits a well-known blue-light photoreceptor, YtvA from *Bacillus subtilis*, and the cyanobacterial phytochrome Cph1 as actinometers. The former is an *ad hoc* developed, four laser-based set up where two cw lasers provide the pump beams to induce photoswitching (red to green and green to red, respectively) and two cw lasers simultaneously monitor the appearance and disappearance of the two species. Interestingly, fit analysis of the recorded transient absorbance changes provided a quantum yield for the green → red conversion (≈0.3), at least three times larger than for the red → green conversion (≈0.08). These data are in agreement with the results from the comparative method, documenting the usefulness of the here developed 'direct' method for quantum yields determination. The light-induced switching capability of this photochromic protein allowed measuring the kinetics of GAF3 immobilized on a glass plate, and within living, overexpressing *Escherichia coli* cells.

Introduction

Cyanobacteriochromes (CBCRs) constitute a subgroup of photochemically active, bilin-binding proteins.[1, 2] They are structurally and functionally related to the well-characterized canonical and bacterial phytochromes, they also bind covalently- via reaction to a conserved cysteine-phycocyanobilin (PCB) as chromophore within a GAF (cGMP-specific phosphodiesterases, Adenylyl cyclases and FhlA)[3] domain, and they undergo photochemical reactions that cause photochromic changes of their absorption maxima. In contrast to canonical phytochromes, however, CBCRs show several significantly different properties. In contrast to plant phytochromes in which a PAS-GAF-PHY (PAS = Per Arnt Sim; PHY = domain named after phytochrome) arrangement of protein domains is instrumental for the preservation of the spectral properties,[4] most CBCRs identified so far show tandem arrays of GAF domains, out of which one or even more have the autonomous capability to covalently bind PCB as chromophore,[5] but even CBCRs carrying a single GAF (with capability of binding bilins) with well established photochromic properties have been reported, e.g. TePixJ. [6] The lyase function is present even when the CBCR-GAF domains are separately expressed as autonomous proteins.

Most interestingly, CBCR-GAF domains show a much wider range for the absorbance maxima of their parental and photoproduct states in contrast to canonical phytochromes that show a red-/far red-absorbance switch (λ_{max} = 660 nm, 710-730 nm for P_R and P_{FR}, respectively, where P_R = red absorbing form and P_{FR} = far red absorbing form). The majority of the CBCR-GAF domains studied so far are generated in a red-absorbing form (GAF_R, λ_{max} around 640 nm), carrying their PCB chromophore in a *Z,Z,Z,s,s,a* configuration. Photoconversion of the parental form, however, yields a great variety of absorbance maxima for the photoproducts of various CBCR-GAF domains, such as red- (λ_{max} around 690 nm), orange- (λ_{max} around 580 nm), green- (λ_{max} around 540 nm), teal- (λ_{max} around 500 nm), and even blue-(λ_{max} around 410 nm) absorbing species.[5, 7, 8] The spectral variance is even further extended, as some GAF domains show a remarkable chemical reactivity: they convert the incorporated PCB chromophore into Phycoviolobilin (PVB)

which reduces the conjugated π-system to only three of the four pyrrole rings.[9] Furthermore, some other GAF domains convert reversibly-after photochemical generation of the photoproduct-their PCB- or PVB-chromophore through the nucleophilic attack of a second cysteine into bili-rubinoid chromophores, then showing absorbance maxima reaching as far as the near UV range, and even a second cysteine linkage present in both inconvertible states has been reported. For more detailed discussion of these unprecedented photochemical properties see refs [10, 11]

CBCR-GAF domains show a moderate, but noticeable fluorescence quantum yield (Φ_F), interestingly for both their parental and photoproduct form of up to 0.1, whereas the corresponding parameter for the canonical phytochromes is negligibly small (Φ_F ca. 10^{-4}).[12, 13] These Φ_F taken together with the large extinction coefficients of 50-80,000 M^{-1} cm^{-1} yield brightness values comparable to most of the fluorescent proteins so far in use.

Considering the photo-switchable absorbance and fluorescence properties, the small size of slightly more than 100 amino acids, the autonomous lyase function, and the wide range of absorbance maxima of CBCR-GAF domains, these proteins might serve as interesting tools in modern microscopic applications (e.g., FLIM, FPALM), similarly as was recently demonstrated for the blue light-sensing, flavin binding receptors. [14] According to their function as photosensory pigments, CBCRs carry a signaling domain, in most cases known so far a functionally proven histidine kinase [7] or a GGDEF-/EAL tandem motif (diguanylate cyclase and phosphodiesterase domains, named after conserved amino acids)[3, 15] akin canonical phytochromes, therefore they might also be considered for experiments in optogenetics.[16]

Astonishingly, relatively few spectroscopic analyses addressing the dynamics of CBCR-GAFs have been performed so far that expand further than the mere determination of their steady state absorbance and fluorescence properties. [17-21] Detailed studies on the ultrafast processes have been provided by the Larsen/Lagarias group. [17, 21] Also, work elucidating the protein structure is still sparse.[10, 22-24] One major parameter for future employment of CBCR-GAF domains is the determination of their photochemical quantum yield that so far has not been addressed quantitatively.

In this work we report novel photophysical and photochemical data for the GAF3 domain of the Slr1393 protein from *Synechocystis* sp. PCC6803. Slr1393 is a 974 aa protein built with, sequentially from the N-terminus, three GAF, one PAS and one histidine kinase domain. The third GAF domain (here referred to as GAF3) is the sole one in Slr1393 that is able to hold PCB as chromophore.[7] Here the determination of red→green and green →red photoconversion quantum yields for GAF3 was achieved by means of two different methods, one of which employs a designed four beam setup that does not need a reference compound as actinometer. Using fluorescence microscopy we also show that photoconversion is maintained in immobilized proteins and in proteins expressed in *E. coli*, an important aspect for biophysical applications.

Experimental

Sample preparation

Generation of recombinant proteins. Heterologous expression of *Synechocystis* proteins Cph1Δ2 and GAF3 of Slr1393 was performed as recently described.[19] A clone encoding Cph1 was kindly provided by Dr. J. Hughes (Univ. Gießen). Both proteins were furnished with PCB as chromophore *in vivo*, using a two plasmid approach.[7] Transformed *E. coli* cells were grown under routine conditions and protein expression was induced by IPTG following standard protocols. For lysis, suspension of centrifuge-harvested cells was added dropwise into liquid nitrogen, and the solid-frozen cell suspension was broken by an Ultra-Turrax in liquid N_2. After evaporation of nitrogen, the centrifugation-cleared supernatant of the cell lysates wase loaded onto an IMAC column and the proteins were purified by stepwise elution with imidazole. While Cph1 was eluted in nearly pure, fully chromophore-loaded form, GAF3 was further passed over an anion-exchange column (DEAE Sephadex, GE healthcare) resulting in removal of most of the non-chromophore-loaded protein. This procedure yielded GAF3 as ca. 70% PCB-loaded protein. Full photochemical reversibility and thermal stability of the photoproduct, as formerly described were documented prior to further experiments. The protein was stored in a Tris buffer (50 mM, pH = 8, 200 mM NaCl, supplemented with 5% glycerol). The protein YtvA was prepared as previously described:[25] following expression in *Escherichia coli* BL21 cells (induction by 0.4 mM isopropyl-β-d-thiogalactopyranoside), the His-tagged protein was purified via affinity chromatography (Ni- IMAC column, 4°C) with gradient elution (10–200 mM imidazole); after imidazole removal, the samples were stored in sodium-phosphate buffer (10 mM NaCl, 10 mM sodium phosphate, pH 8.0). Zinc phthalocyanine was purchased from Sigma-Aldrich.

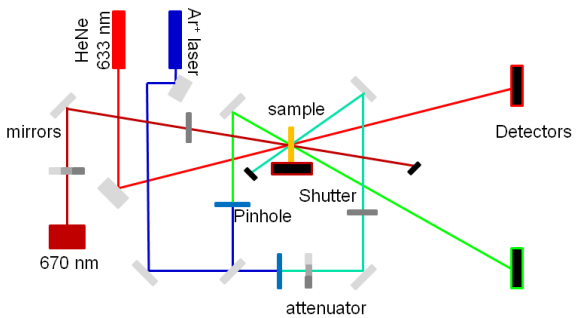

Figure 1 Schematic presentation of the experimental setup for the photoconversion experiments.

Photoconversion experiments using an actinometer

For photoconversion of YtvA we employed a Led-Lenser®V8 lamp (Zweibrüder Optoelectronics, Solingen-Germany), emitting with a maximum at 462 nm and a 25 nm half-width (LED462). Maximal photoconversion of Cph1 (Red/FarRed absorbing forms) and complete conversion of GAF3 (Red/Green absorbing forms) were achieved by means of a diode laser (670 nm, for $Cph1_{R\rightarrow FR}$ and $GAF3_{R\rightarrow G}$), and 25 nm half-width LEDs emitting with maxima at 720 nm ($Cph1_{FR\rightarrow R}$) and 530 nm ($GAF3_{G\rightarrow R}$). Absorption spectra were recorded with a Jasco 7850 UV/Vis spectrophotometer. Steady-state fluorescence measurements and partial photoconversion to evaluate photoconversion quantum

yields, were carried out with a Perkin-Elmer LS50 luminescence spectrometer (Perkin-Elmer Ltd,. Beaconsfield, England).

Laser induced photoconversion experiments

Photoconversion of GAF3 solutions was induced by a dedicated experimental setup (Figure 1) using either a diode laser (670 nm) or the 488 nm emission of a multiline, continuous-wave argon ion laser (JDS Uniphase 150 mW all lines). The resulting absorbance changes were monitored using a split portion of the 514 nm line (100 µW) of the same argon ion laser and the attenuated output at 633 nm of a He-Ne laser (40 µW). The 488 and 514 nm lines were separated by a Pellin Broca prism and selected through iris diaphragms. The power of the pump beams was varied using a variable attenuator (Thorlabs) and measured directly by a power meter (Thorlabs) equipped with a pyroelectric energy probe. Experiments were conducted as a function of pump laser power between 17 and 0.28 mW at 488 nm, and between 1.88 and 0.7 mW at 670 nm. In order to prevent a relevant contribution of diffusion to the measured kinetics, the excitation beam at 670 nm was used unfocused and the 488 nm line was shaped by means of a beam expander. Therefore, the pump lasers hit a relatively large sample area, circular (15 mm diameter) for the 488 nm and rectangular for 670 nm (16×8 mm), containing the spot illuminated by the probe beam (1 mm diameter). Two preamplified Si photodiodes were used to monitor the transmitted light intensity at 514 nm and 633 nm. Fluorescence emission was collected at right angle from excitation beams with a photomultiplier (Hamamatsu H5784-04) through a cutoff, long-pass filter (> 670 nm). The time course of the signal was digitized with a digital oscilloscope (LeCroy Waverunner 104-Xi) and transferred to a computer for further analysis. Two fast mechanical shutters (Uniblitz) were positioned on the path of the pump lasers before the sample holder and allowed exposure of the samples to the 488 nm and 670 nm beam to achieve green → red and red → green conversion, respectively. Exposure times were selected by means of the shutter drivers (Uniblitz). The sample holder (Flash 300, Quantum Northwest) was accurately temperature-controlled at 20°C with a Peltier element, allowing a temperature stability of better than 0.1°C.

Photoconversion of immobilized GAF3 proteins and of GAF3 within bacterial cells

Images were acquired on an inverted fluorescence microscope (Nikon Eclipse TiE/B) equipped with a 100x 1.4 NA Nikon objective lens and a back-illuminated electron-multiplying charge-coupled device (CCD) camera (Andor Ixon DU-897E-CS0BV) running at 20 Hz (50 ms exposure time). The laser lines used to switch between the green and red form were the 647 nm (red-to-green photo-conversion, Coherent CUBE 647 nm) and the 488 nm (green-to-red photo-conversion, Coherent Sapphire OPSL 488 nm) both coupled into a collinear path by a dichroic filter (Chroma Tech. F43-491). The power range used to record the fluorescence kinetics of GAF3 both in the dried monolayer and inside *E. coli* was between 0.12 - 0.70 mW for the 647 nm line and 0.13 – 1.15 mW for the 488 nm line (FWHM of the excitation intensity distribution of 35±1 µm for 647 nm and of 52±2 µm for 488 nm). In order to optimize the decoupling of the emission of the two species, the detection bandwidth (dichroic mirror DM660 and band-pass dichroic filter Semrock BP-705\72) was limited to the end of the emission spectrum, where the green and red fluorescence show the highest degree of separation.

The fluorescence measurements were performed both on a dry layer of purified protein GAF3 and on *E. coli* cells overexpressing the photochromic domain. Cultures of the transformed *E. coli* cells were grown overnight in LB medium and appropriate antibiotic selection at 37°C with aeration. Day cultures were inoculated to an optical density of 0.01-0.05 at 600 nm (OD_{600}) in LB medium with antibiotics at 37°C with aeration until they reach an OD_{600} 0.3-0.6 (mid-exponential phase). Protein expression was induced by adding 25 µM IPTG for 3 h. To avoid contamination by LB fluorescence during the measurement, the samples were centrifuged at 2,000 rpm for 3 min each and the pellet was resuspended in M9 minimal salts. A 5µl drop of the concentrated culture was spotted onto a round coverslip and then immobilized by placing a thick agar pad on top of the bacteria. This configuration also allows keeping the culture hydrated for a longer period.

Results and Discussion

Photochromic properties

GAF3 undergoes a red/green photochemistry, as previously shown[19] and illustrated in Figure 2. Red light illuminating of GAF3 leads to formation of a green absorbing species, $GAF3_G$, showing a broad band centered at 535 nm. Conversely, illumination with green light leads to formation of a red absorbing species, $GAF3_R$, with a peak around 650 nm and a shoulder at 590 nm. Upon excitation of the red-absorbing species at the isosbestic point at 580 nm, a band at 675 nm is observed in the fluorescence emission spectrum. Excitation of the green-absorbing species at 580 nm results in a much weaker and broad fluorescence emission with a maximum at 635 nm.

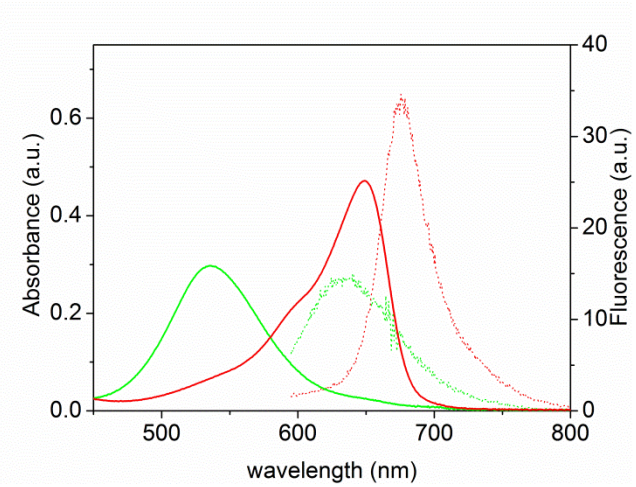

Figure 2 Steady state absorbance (solid lines) and fluorescence emission (dotted lines) spectra of Slr1393 from *Synechocystis* sp. PCC6803 of the red-absorbing species (red) and green-absorbing species (green). Fluorescence excitation was at 580 nm (isosbestic point).

Fluorescence quantum yield

The fluorescence quantum yield of $GAF3_R$ was determined as $\Phi_{F,R} = 0.1$, using Zn-phthalocyanine as a standard ($\Phi_F = 0.3$ in benzene [26] and 610 nm excitation, and correcting for the different

refraction index of the solvents). For GAF3$_G$, $\Phi_{F,G}$ = 0.06 was measured by comparison with GAF3$_R$, exciting both forms at the isosbestic point, equal to 580 nm. Given that GAF3$_G$ can be partially photoconverted to GAF3$_R$ during fluorescence measurements (*vide infra*), the sample was kept illuminated with a LED emitting at 670 nm. The obtained values are slightly higher than those previously determined using phycocyanin as a standard (0.06 and 0.03 for GAF3$_R$ and GAF3$_G$ respectively). [7] However, in order to test the reliability of our estimation, we have measured Φ_F of the red-light absorbing state of Cph1 using GAF3$_R$ as a standard ($\Phi_{F,R}$ = 0.1) and we obtained a value of 0.023, in agreement with the value reported in the literature (0.024). [27]

Laser photoconversion experiments

The photoisomerization quantum yields, denoted as Φ_{RG} (red→green) and Φ_{GR} (green→red), are the most important parameters for photochromic molecules like GAF3 domains, because they measure the efficiency of the nonradiative decay channel(s) that lead to the stereochemical changes upon light absorption.[28]

With the aim to determine Φ_{RG} and Φ_{GR}, we arranged a dedicated experimental set up, based on four cw laser beams, two for the excitation of the GAF3 domain and two for the monitoring of the photoconversion (see Experimental Section for details). A standard comparative method that exploits an actinometer as a reference with well-established photoconversion quantum yield was used to validate the methodology (see below).

A typical set of signals detected in these experiments is shown in Figure 3. Illumination with the diode laser at 670 nm or the 488 nm line of the argon ion laser allowed achieving red → green or green → red conversion, respectively. The absorbance changes at 514 nm (green line) and 633 nm (red line) allowed monitoring simultaneously the appearance or the disappearance of each species. Importantly, the time profile of the fluorescence emission perfectly matches the absorbance changes (see inset to Figure 3 for an example).

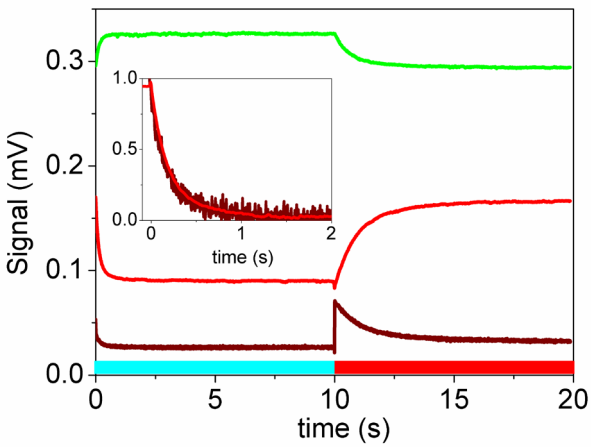

Figure 3 Cyclic photoconversion of GAF3 between green and red absorbing species, after illumination with the 670 nm output (1.88 mW) of a diode laser or the 488 nm line (11 mW) of an argon ion laser, monitored through transmitted intensity change at 633 (red line) or 514 nm (green line). Fluorescence emission collected at right angle from excitation through a lowpass filter is shown as the dark red line. The cyan and red bars indicate illumination periods with the beams at 488 and 670 nm, respectively. T=20°C. INSET: comparison between the red→green photoconversion as monitored by normalized changes in absorbance at 633 nm (red) and fluorescence emission (dark red).

Figure 3 and analyses of those traces demonstrate that kinetics are essentially the same at both observation wavelengths. In order to minimize artifactual photoconversion by probe beams, kinetics reported in the following were collected using only the 633 nm monitoring beam, which proved to affect minimally the measured kinetics (see below). Moreover, it is important to note that data collected in different illumination cycles demonstrated a remarkably high stability of the chromophore towards photobleaching in the employed fluence range.

Following the kinetics of red → green and green → red conversion as a function of pump laser power allowed us to estimate the reaction quantum yields. [28] Figure 4 shows the absorbance changes resulting from green → red (Figure 4a) and red → green (Figure 4b) conversion monitored at 633 nm at selected pump laser power values. All curves are well described by exponential decay functions and the rate constants retrieved from the fitting show the expected linear dependence on pump laser power (Figures 4c and 4d). However, for the red → green photoconversion the observed rate constant extrapolates to a finite value at zero laser power (Figure 4d). This results from background red → green photoconversion due to the probing beam at 633 nm, whose low power is nevertheless high enough to result in an appreciable photoconversion rate. This effect was not so evident in the green → red photoconversion because of the much higher (tenfold) laser power of the green beam. This parasite effect leads to an apparent increase in the conversion rate constant which we took into account in the analysis reported below. Fluorescence emission by GAF3 solutions excited either at 670 or 488 nm from the photolysis beams, and collected at right angle from excitation through a lowpass filter (cutting at 670 nm), showed a decrease in intensity from their initial values as a function of time, as reported in Figure 3. Inset to Figure 3 demonstrates that the changes in absorbance and fluorescence during green → red photoconversion, induced by 488 nm light, proceed with the same kinetics.

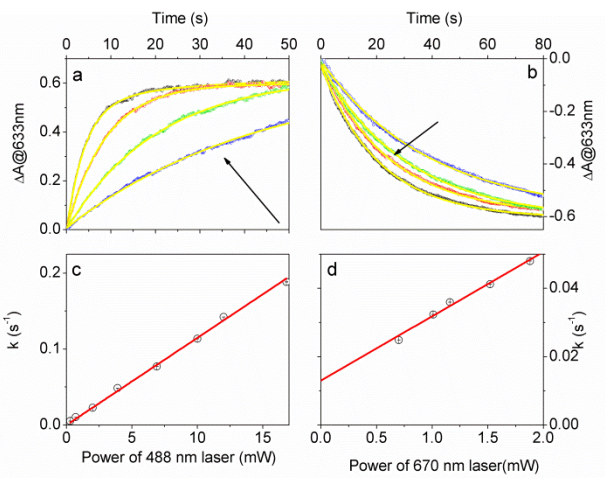

Figure 4 Panel a and b. Transient absorbance changes of GAF3 in buffered solution (open circles) upon excitation with 488 nm laser (panel a) and 670 nm (panel b) at increasing power between 0.3 and 16.8 mW

and between 0.7 and 1.9 mW, respectively. The arrow indicates increasing laser power. Yellow solid lines result from the fitting with an exponential decay function. T = 20 °C. Panel c and d. Dependence of rate constants for the green → red (c) and red → green (d) conversion as a function of pump laser power (488nm, c; 670nm, d). Rate constants were retrieved as k=1/τ, resulting from the exponential decay fitting.

A similar agreement is observed for the red → green photoconversion induced by 670 nm light, indicating that the kinetics observed through fluorescence emission are directly associated with the photoconversion process. Figure 5 displays kinetics collected under 670 nm illumination at selected laser power values. The decrease in fluorescence becomes faster as the laser power is increased and shows monoexponential relaxation. The laser power dependence of the apparent relaxation rate shows a linear trend. Unlike for the absorbance changes (Figures 3 and 4), the fluorescence emission intensity shows invariably a decrease for both photoconversions. The fluorescence emission excited by 488 nm photoconversion shows the same general trend but displays a poor signal to noise ratio. This can be rationalized on the basis of the changes in the molar extinction coefficients, fluorescence quantum yields and spectral emission distributions of the two species. Fluorescence emission changes after photoexcitation of GAF3$_G$ at 488 nm are expected to be lower than those observed after 670 nm excitation of GAF3$_R$ which can be ascribed to a combination of the 3.9-fold lower molar extinction coefficient at the excitation wavelength (at 488 nm ε_G ca. 15,000 M^{-1} cm^{-1} and ε_R ca. 3,900 M^{-1} cm^{-1}), the 1.67-fold increase in the fluorescence emission quantum yield ($\Phi_{F,R}$ = 0.1 and $\Phi_{F,G}$ = 0.06), and a change in the overlap between the fluorescence emission spectra of GAF3$_G$ and GAF3$_R$, and the transmission curve of the emission filter, responsible for a 1.86-fold increase in sensitivity. Taking together these various parameters this leads to a nearly 20% decrease in the fluorescence emission observed for a pure GAF3$_G$ solution. In the case of the 670 nm photoexcitation, the change in molar extinction coefficient is from ε_G = 2,243 M^{-1} cm^{-1} to ε_R = 33,230 M^{-1} cm^{-1}, resulting in an overall decrease of 98%. Similar effects are estimated when 647 nm excitation is used in the experiments reported in Figure 8 on immobilized proteins and on proteins expressed in *E. coli* (Figure 10, see below).

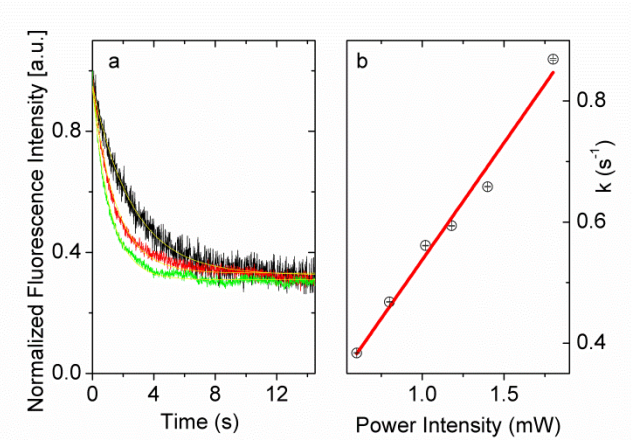

Figure 5 Panel a: fluorescence emission intensity for a GAF3 solution as a function of time excited after excitation at 670 nm collected at right angle from excitation beam after passing through a lowpass filter (cutting below 670 nm) at some selected pump laser powers (0.6 mW (black); 1.4 mW (red) and 1.8 mW (green)). Panel b shows the laser power dependence of the apparent rate determined from exponential fitting of the decay curves (yellow lines in the upper panel).

Determination of photoconversion quantum yields

Photoconversion yields can be calculated considering that the concentrations of GAF3$_R$ and GAF3$_G$ species are readily determined from a simple balance between rates for forward and reverse photoreactions induced by photons of energy $h\nu$ (h = Planck's constant, ν = frequency of the photons):

$$GAF3_R \underset{h\nu green,\Phi_{GR}}{\overset{h\nu red,\Phi_{RG}}{\rightleftharpoons}} GAF3_G \qquad (1)$$

In this kinetic scheme Φ_{RG} and Φ_{GR} represent the forward and reverse reaction yields, respectively. Thermal relaxations in either direction are neglected in view of their very small contribution, as demonstrated by steady-state measurements, which revealed that the red and the green absorbing species are stable for hours in the dark (data not shown).

Following the procedure previously described,[14, 28] the experimental data were fitted using the solutions of the differential equations associated with the kinetic scheme (Figure 6). They describe the temporal evolution of the molar concentrations of the two molecular species GAF3$_R$ and GAF3$_G$. The concentrations of GAF3$_R$ and GAF3$_G$ are indicated as R=[GAF3$_R$], G=[GAF3$_G$], GAF3$_{tot}$ is a constant equal to [GAF3$_R$]+[GAF3$_G$]. Taking into account the conversion induced by the pump laser beam (alternatively 488 or 670 nm) and the monitoring red laser beam, the rate of change in R and G can be expressed as:

$$\begin{cases} \dfrac{dR}{dt} = \dfrac{P^{pump}}{V}\ln 10\left(A_G{}^{pump}\Phi_{GR} - A_R{}^{pump}\Phi_{RG}\right) + \dfrac{P^{633}}{V}\ln 10\left(A_G{}^{633}\Phi_{GR} - A_R{}^{633}\Phi_{RG}\right) \\ \dfrac{dG}{dt} = -\dfrac{dR}{dt} \end{cases} \qquad (2)$$

where P^{pump} and P^{633} are the powers of the light beams (in Einstein/s), V is the illuminated volume, $A_R{}^{pump}$ and $A_G{}^{pump}$ are the absorbances at the excitation wavelengths (488 nm or 670 nm), $A_R{}^{633}$ and $A_G{}^{633}$ at the probing wavelength (633 nm) of GAF3$_R$ and GAF3$_G$, respectively. Obviously $A_X^{\lambda} = [X]\varepsilon_X^{\lambda}\ell$ (where X = R or G, λ is the wavelength of the light beam, ℓ is the light beam path along the solution). Considering that the concentrations R and G are not linearly independent, we can simplify the rate equation and solve only the one for GAF$_R$. Then, using the Lambert-Beer law, each kinetics can be described by:

$$\frac{dA}{dt} = \varepsilon_R^{633}\ell\frac{dR}{dt} + \varepsilon_G^{633}\ell\frac{dG}{dt} = (\varepsilon_R^{633} - \varepsilon_G^{633})\ell\frac{dR}{dt} \qquad (3)$$

The global fitting of the laser photoconversion traces recorded at several illumination powers afforded Φ_{RG} = 0.08±0.01 and Φ_{GR} = 0.30±0.02 (pump at 488 nm) and Φ_{RG} = 0.09±0.01 and Φ_{GR} = 0.31±0.02 (pump at 670 nm), perfectly consistent with the determination from the steady state data (see below). The analysis of the kinetics consistently indicates that the photochromic transformation of GAF3$_G$ into GAF3$_R$ occurs in higher yield than the reverse GAF3$_R$ → GAF3$_G$ reaction. The behavior of GAF3 is remarkably different from that of canonical phytochromes, for which the forward and reverse photoreactions are characterized

by the same quantum yield (ca. 0.15-0.17).[29, 30] This finding is consistent with the results obtained on NpR6012g4 and NpF2164g6 from *Nostoc punctiforme*, for which different photoconversion yields were determined for forward and reverse photoconversions. [31]

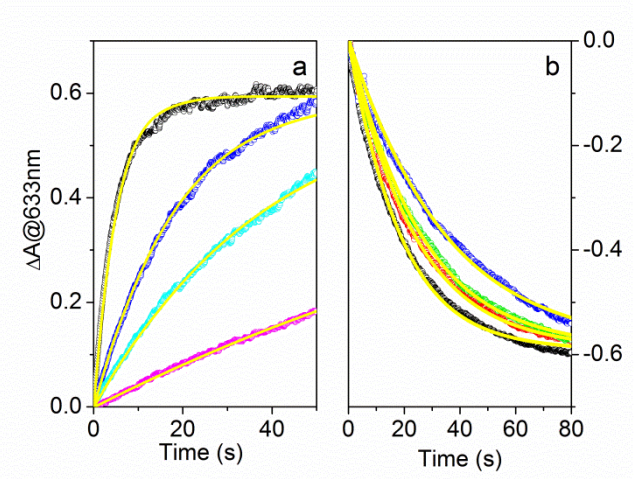

Figure 6 Results of global analysis of selected data obtained upon excitation with 488nm laser (Panel a) and 670 nm (Panel b) at increasing power (Panel a: 16.8 mW (black); 3.9 mW (blue); 2 mW (cyan); 0.7 mW (magenta); Panel b: 1.88 mW (black); 1.52 mW (red); 1.16 mW (green); 0.7 mW (blue)).

Photochemical quantum yields using reference compounds

The value of Φ_{RG} for GAF3 was also determined using Cph1 as actinometer ($\Phi_{R/FR}$ for Cph1 = 0.16).[30] Photoconversion was achieved through irradiation of the sample at 650 nm with the fluorometer excitation light source. Absorption spectra were then recorded at increasing exposure times. The fluorometer light intensity is sufficiently strong for partial photoconversion of the $GAF3_R$ and $Cph1_R$ to the $GAF3_G$ and $Cph1_{FR}$ forms, respectively (Figure 7).

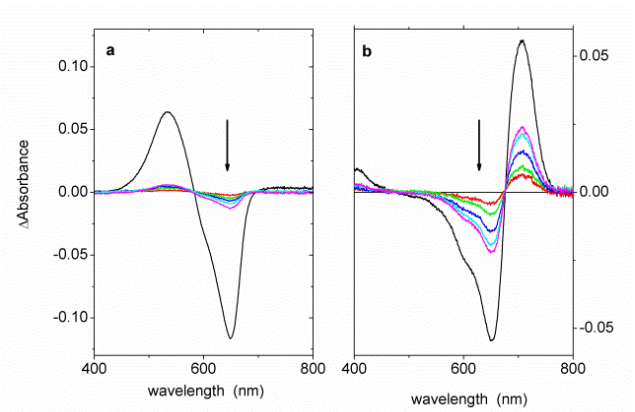

Figure 7 Difference absorption spectra recorded after 500 s illumination steps (total =2550) at 650 nm, starting for the "red" forms of GAF3 (a) and Cph1 (b). The arrow's direction indicates increasing illumination times. Black lines refer to the fully photoconverted forms, i.e. $GAF3_G$-$GAF3_R$ and $Cph1_{FR}$-$Cph1_R$. T = 20 °C.

Given the fact that $GAF3_R$ and $Cph1_R$ have the same absorption coefficient at 650 nm within the experimental accuracy, [13] we obtained a value of Φ_{RG} = 0.09 by comparing the slopes of the two linear plots ΔAbs_{650} vs. irradiation time (data not shown). Thermal reversion can be neglected in both cases (data not shown), as well as contribution of the photoproducts to the observed ΔAbs_{650}, also given the very small photoconverted fraction during 2500 s of irradiation.

The value of Φ_{GR} for GAF3 is more difficult to determine, given the lack of suitable reference compounds in the green region of the spectrum. In this case we employed the flavin-binding photoreceptor YtvA (λ_{max} = 447 nm), for which the quantum yield of formation of the photoproduct is Φ_{390}=0.49. [32] We have applied a similar protocol as the one outline above, where we irradiated the proteins with the 488 nm output from the fluorometer. In this case, we recorded the differential absorbance at 474 nm for YtvA and at 650 for GAF3 for a total 2500 s irradiation in steps of 500 s. After correcting for the different absorption coefficients, we obtained Φ_{GR} = 0.24. This value might be overestimated, given that a partial thermal recovery for YtvA occurs under these conditions. [14] Alternatively, we illuminated both compounds for 40 s with LED462, in 10 s steps: comparing the photoconversion rates, we obtained a value of 0.18 for Φ_{GR}. (data not shown). With this second methodology, problems may arise from the 25 nm emission bandwidth of the LED, highlighting the importance of a method for absolute quantum yields determination, without the need of a reference compound. In summary, the comparative methodology gives values of Φ_{RG} =0.09 and Φ_{GR} = 0.18-0.24. This result confirms the finding that the $GAF3_G \rightarrow GAF3_R$ reaction occurs in significantly higher yield than the $GAF3_R \rightarrow GAF3_G$ reaction.

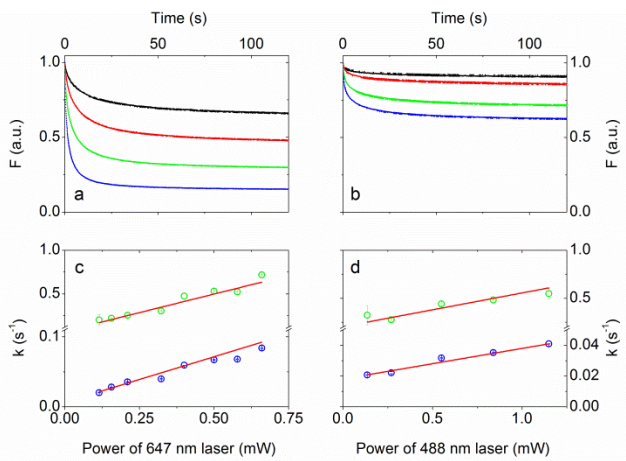

Figure 8. Fluorescence emission intensity for a GAF3 layer deposited on a glass plate, as a function of time after excitation at 647 nm (a) and 488 nm (b) at an intensity range of 0.11-0.66 mW and 0.13-1.15 mW, respectively. Panels c and d show the laser power dependence of the apparent rates determined from double exponential fitting of the decay curves.

Photoconversion of immobilized GAF3

Similarly as performed with GAF3 solutions, we have studied photoconversion of GAF3 proteins immobilized on a glass plate by monitoring their fluorescence emission. Figure 8 shows the changes in fluorescence emission collected through the microscope objective after photoconversion at 488 nm or 647 nm. While the pattern is similar to that shown for GAF3 solutions, the kinetics in this case is best described by a double exponential relaxation. The reason for the non-exponential decay is not yet

clear, but it seems reasonable to suggest an effect of protein hydration as observed for other immobilized proteins.[33-35] Alternatively, one might assume that photobleaching becomes relevant under the experimental conditions inside the microscope, where laser fluence is higher than that normally used in experiments on bulk solutions. As observed for the GAF3 solutions, the fluorescence emission decreases from the initial value in both photoconversion processes. This decrease is larger for 647 nm excitations, leading to almost full disappearance of the fluorescence emission. As discussed above, 488 nm induced photoconversion leads to a much smaller decrease in fluorescence emission due to the residual excitation of the red species by the blue light and the strong overlap of fluorescence emission of the two species. The present data demonstrates that the photochromic properties of GAF3 are preserved also when immobilized in a dry film, although from the fluorescence emission it appears difficult to assess whether the photoconversion yields are affected by the environment and to what extent.

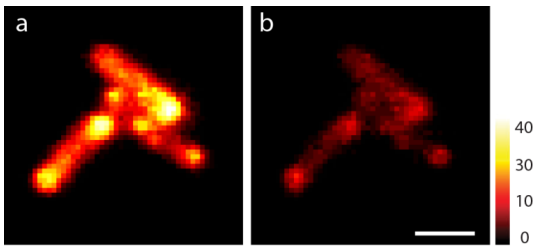

Figure 9 Transformed *E. coli* cells overexpressing GAF3 were excited at 647 nm (panel a) and 488 nm (panel b) and fluorescence was detected in the red portion of the emission spectrum (See Experimental section). Scale bar 2 µm.

Photoconversion in GAF3 overexpressing *E. coli* cells

Above described photochromicity and fluorescence emission of GAF3 led us to study the properties of GAF3 within living cells. To this purpose transformed *E. coli* cells were induced to overexpress GAF3 and the resulting fluorescence emission was monitored. Figure 9 shows images collected with a fluorescence widefield microscope, where the fluorescence emission from GAF3 appears to be unevenly distributed, with accumulation of fluorophores at the tips of the bacteria. In order to check whether the photoreceptor undergoes photochromic transformations, fluorescence intensity was detected as a function of time after excitation at 488 nm or 647 nm. Results were independent of the specific spot selected on the image.

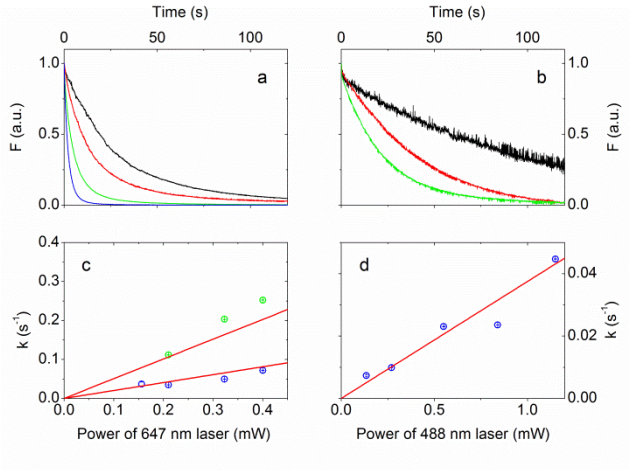

Figure 10 Fluorescence emission intensity for GAF3-overexpressing *E. coli* cells as a function of time after excitation at (a) 670 nm and (b) 488 nm intensity range of 0.15-0.5 mW and 0.13-1.15 mW, respectively. Panels c and d show the laser power dependence of the apparent rates determined from exponential fitting of the decay curves.

The GAF3$_R$ → GAF3$_G$ photoconversion kinetics measured for proteins inside *E. coli* is best described by a biexponential relaxation, whereas the reverse photoreaction can be fitted with a single exponential decay (Figure 10). The present results demonstrate that the photochromic behavior of GAF3 is preserved also for proteins inside living cells, although a quantitative characterization of the reaction yields in these conditions appears beyond the capabilities of the present analysis. Figure 9 shows that the fluorescence emission excited by 488 nm excitation occurs with lower yield than under 647 nm excitation. However, given the strong overlap between the emission of GAF3$_R$ and GAF3$_G$ and the substantial overlap of the excitation of the two species in the green region, it proved impossible to turn completely off the emission. Thus, in our experiments it appears difficult to achieve a regime in which fluorescence by a sparse subset of single molecules[36] is restored by selective photoactivation.

Conclusions

Photochromic conversion of GAF3$_G$ into GAF3$_R$ and vice versa can be repeatedly achieved using alternatively green and red light irradiation. However, unlike canonical phytochromes, photoconversion of GAF3$_G$ into GAF3$_R$ occurs in higher yield than the opposite reaction. The photochromic transformation is also detectable through the distinct fluorescence emission by the two species, but the strong overlap of their fluorescence emission and the overlapping excitation spectra in the blue-green range appear to limit the contrast attainable in microscopy applications. Development of mutants with shifted fluorescence emission band for one of the species may allow improving contrast and thus exploit this novel class of proteins in microscopy methods exploiting stochastic activation of single molecules.

Notes and references

[a] *Fondazione Istituto Italiano di Tecnologia, via Morego 30, 16163 Genova, Italy*
[b] *Dipartimento di Fisica e Scienze della Terra "Macedonio Melloni", Università di Parma, viale delle Scienze 7/A, 43124, Parma, Italy*

[c] *Max-Planck-Institute for Chemical Energy Conversion, Stiftstrasse 34-36, D-45470 Mülheim, Germany*
[d] *State Key Laboratory of Agricultural Microbiology, Huazhong Agricultural University, Wuhan 430070, PR China*
[e] *NEST, Istituto Nanoscienze-CNR*
[f] *Nikon Imaging Center, Fondazione Istituto Italiano di Tecnologia, via Morego 30, 16163 Genova, Italy*
[g] *Dipartimento di Bioscienze, Università di Parma, viale delle Scienze 11/A, 43124, Parma, Italy. Tel +390521905208, fax +390521905223, Email: stefania.abbruzzetti@unipr.it*

Acknowledgements

This work was partially supported by MIUR National program PRIN 2010JFYFY2_002.
X.X. is grateful for a research grant from the exchange program of the Chinese Academy of Sciences and the Max-Planck-Society. W.G. wishes to thank the Max-Planck-Society for continuous generous support.

References

1. M. Ohmori, M. Ikeuchi, N. Sato, P. Wolk, T. Kaneko, T. Ogawa, M. Kanehisa, S. Goto, S. Kawashima, S. Okamoto, H. Yoshimura, H. Katoh, T. Fujisawa, S. Ehira, A. Kamei, S. Yoshihara, R. Narikawa and S. Tabata, *DNA Research*, 2001, **8**, 271-284.
2. M. Ikeuchi and T. Ishizuka, *Photochemical & Photobiological Sciences*, 2008, **7**, 1159-1167.
3. P. Jones, D. Binns, H.-Y. Chang, M. Fraser, W. Li, C. McAnulla, H. McWilliam, J. Maslen, A. Mitchell, G. Nuka, S. Pesseat, A. F. Quinn, A. Sangrador-Vegas, M. Scheremetjew, S.-Y. Yong, R. Lopez and S. Hunter, *Bioinformatics*, 2014, **30**, 1236-1240.
4. S. Sharda, R. Shah and W. Gärtner, *Eur. Biophys. J.*, 2007, **36**, 815-821.
5. R. Narikawa, Y. Fukushima, T. Ishizuka, S. Itoh and M. Ikeuchi, *J. Mol. Biol.*, 2008, **380**, 844-855.
6. T. Ishizuka, T. Shimada, K. Okajima, S. Yoshihara, Y. Ochiai, M. Katayama and M. Ikeuchi, *Plant and Cell Physiology*, 2006, **47**, 1251-1261.
7. Y. Chen, J. Zhang, J. Luo, J.-M. Tu, X.-L. Zeng, J. Xie, M. Zhou, J.-Q. Zhao, H. Scheer and K.-H. Zhao, *FEBS J.*, 2012, **279**, 40-54.
8. G. Enomoto, Y. Hirose, R. Narikawa and M. Ikeuchi, *Biochemistry*, 2012, **51**, 3050-3058.
9. T. Ishizuka, A. Kamiya, H. Suzuki, R. Narikawa, T. Noguchi, T. Kohchi, K. Inomata and M. Ikeuchi, *Biochemistry*, 2011, **50**, 953-961.
10. E. S. Burgie, Joseph M. Walker, George N. Phillips Jr and Richard D. Vierstra, *Structure*, 2013, **21**, 88-97.
11. N. C. Rockwell, S. S. Martin, K. Feoktistova and J. C. Lagarias, *Proc. Natl. Acad. Sci. USA*, 2011, **108**, 11854-11859.
12. H. Brock, B. P. Ruzsicska, T. Arai, W. Schlamann, A. R. Holzwarth and S. E. Braslavsky, *Biochemistry*, 1987, **26**, 1412-1417.
13. J. Zhang, X.-J. Wu, Z.-B. Wang, Y. Chen, X. Wang, M. Zhou, H. Scheer and K.-H. Zhao, *Angew. Chem. Int. Ed.*, 2010, **49**, 5456-5458.
14. A. Losi, W. Gärtner, S. Raffelberg, F. C. Zanacchi, P. Bianchini, A. Diaspro, C. Mandalari, S. Abbruzzetti and C. Viappiani, *Photochem. Photobiol. Sci.*, 2013, **12**, 231–235.
15. G. Enomoto, R. Nomura, T. Shimada, N.-N. Win, R. Narikawa and M. Ikeuchi, *J. Biol. Chem.*, 2014.
16. D. Tischer and O. D. Weiner, *Nat Rev Mol Cell Biol*, 2014, **15**, 551-558.
17. P. W. Kim, L. H. Freer, N. C. Rockwell, S. S. Martin, J. C. Lagarias and D. S. Larsen, *Biochemistry*, 2012, **51**, 619-630.
18. Y. Fukushima, M. Iwaki, R. Narikawa, M. Ikeuchi, Y. Tomita and S. Itoh, *Biochemistry*, 2011, **50**, 6328-6339.
19. X.-L. Xu, A. Gutt, J. Mechelke, S. Raffelberg, K. Tang, D. Miao, L. Valle, C. D. Borsarelli, K.-H. Zhao and W. Gärtner, *ChemBioChem*, 2014, **15**, 1190-1199.
20. A. F. E. Hauck, S. J. O. Hardman, R. J. Kutta, G. M. Greetham, D. J. Heyes and N. S. Scrutton, *J. Biol. Chem.*, 2014.
21. P. W. Kim, L. H. Freer, N. C. Rockwell, S. S. Martin, J. C. Lagarias and D. S. Larsen, *J. Am. Chem. Soc.*, 2012, **134**, 130-133.
22. R. Narikawa, T. Ishizuka, N. Muraki, T. Shiba, G. Kurisu and M. Ikeuchi, *Proc. Natl. Acad. Sci. USA*, 2013, **110**, 918-923.
23. E. S. Burgie, A. N. Bussell, J. M. Walker, K. Dubiel and R. D. Vierstra, *Proc. Natl. Acad. Sci. USA*, 2014, **111**, 10179-10184.
24. C. C. Cornilescu, G. Cornilescu, E. S. Burgie, J. L. Markley, A. T. Ulijasz and R. D. Vierstra, *J. Biol. Chem.*, 2014, **289**, 3055-3065.
25. S. Raffelberg, M. Mansurova, W. Gärtner and A. Losi, *J. Am. Chem. Soc.*, 2011, **133**, 5346-5356.
26. A. M. Brouwer, *Pure & Appl. Chem.*, 2011, **83**, 2213-2228.
27. J. Mailliet, G. Psakis, K. Feilke, V. Sineshchekov, L.-O. Essen and J. Hughes, *J. Mol. Biol.*, 2011, **413**, 115-127.
28. V. Voliani, R. Bizzarri, R. Nifosı, S. Abbruzzetti, E. Grandi, C. Viappiani and F. Beltram, *J. Phys. Chem. B*, 2008, **112**, 10714-10722.
29. J. C. Lagarias, J. M. Kelly, K. L. Cyr and W. O. Smith, *Photochem.Photobiol.*, 1987, **46**, 5-13.
30. T. Lamparter, F. Mittmann, W. Gärtner, T. Bärner, E. Hartmann and J. Hughes, *Proc. Natl. Acad. Sci. USA*, 1997, **94**, 11792-11797.
31. C.-W. Chang, S. M. Gottlieb, P. W. Kim, N. C. Rockwell, J. C. Lagarias and D. S. Larsen, *J. Phys. Chem. B*, 2013, **117**, 11229-11238.
32. A. Losi, E. Polverini, B. Quest and W. Gärtner, *Biophys. J.*, 2002, **82**, 2627–2634.
33. S. J. Hagen and W. A. Eaton, *J. Chem. Phys.*, 1996, **104**, 3395-3398.
34. L. Cordone, G. Cottone, S. Giuffrida, G. Palazzo, G. Venturoli and C. Viappiani, *Biochim. Biophys. Acta - Proteins and Proteomics*, 2005, **1749**, 252– 281.
35. F. Pennacchietti, S. Abbruzzetti, A. Losi, C. Mandalari, R. Bedotti, C. Viappiani, F. C. Zanacchi, A. Diaspro and W. Gärtner, *PLoS ONE*, 2014, **9**, e107489.
36. F. Cannone, M. Caccia, S. Bologna, A. Diaspro and G. Chirico, *Microscopy Research and Technique*, 2004, **65**, 186-193.

